Intensity of singular stress field for three-dimensional butt joint to evaluate the adhesive strength

Intensity of singular stress field for three-dimensional butt joint to evaluate the adhesive strength

N-A Noda[1,3], K Tsuboi[1], R Takaki[1], F Ren[1], M R Aridi[1], Y Sano[1], Y Takase[1] and T Miyazaki[2]

[1] Department of Mechanical Engineering, Kyushu Institute of Technology Sensui-Cho 1-1 Tobata-Ku, Kitakyushu-Shi, Fukuoka, Japan
[2] Department of Mechanical Engineering, University of the Ryukyus Azasenbaru 1, Nishihara-Cho, Nakagami-Gun, Okinawa, Japan

E-mail: noda@mech.kyutech.ac.jp

Abstract. Adhesive joints are extensively used in various manufacturing processes in different industrial sectors because of its high fatigue resistance. Different materials properties cause the singular stress field, whose intensity is depending on the adhesive joint geometry. Our previous studies show that debonding strength can be expressed as a constant value of the critical intensity of singular stress field (ISSF) by using two-dimensional butt joint models. By considering real specimen geometry, in this paper, the ISSFs on the interface outer edges of three-dimensional butt joints are analysed by varying the adhesive thicknesses. A mesh-independent technique combined with three-dimensional finite element method (FEM) is shown to evaluate the ISSF. The ISSF distributions on the interface outer edges are analysed in comparison with the previous two-dimensional results. It is found that the critical ISSF considered 3D geometry is almost constant independent of the adhesive thickness.

1. Introduction

Nowadays composite materials become one of the most important structural materials in various industrial fields to replace previous conventional joining technologies. However, different materials properties cause singular stress at the end of the interface, which may lead to failure of bonding portions in structures. Several problems on debonding strength have been studied recently [1-3]. By using butt and single lap joints, the study showed that the tensile strength of the butt joints decreased as adhesive thickness increases while the shear strength did not affected by the adhesive thickness of single lap joints [4]. The same result that related to adhesive strength and adhesive thickness has been observed [5-7]. On the other hand, the study of the effects of surface roughness, adhesive thickness and combined stresses on the adhesive strength for various metals bonded with epoxy resin has been also discussed [8].

Moreover, the experimental studies also justified that the result will be affected by the residual strain of the adhesive layer [9-12]. Suzuki [13] experimentally observed the specimens where S35C JIS medium carbon steel plates are bonded by epoxy resin and it is found that the adhesive strength decreases with increasing adhesive thickness h and tends to be a constant when $h/W \geq 1$, where W is the width of specimen. In addition, Akisanya and Meng [14] discussed the experimental adhesive strength for the butt joints with rectangular cross section. To explain those experimental results, Noda *et al* [15-16] proposed a useful method to calculate the intensity of singular stress field (ISSF) at the

adhesive dissimilar joint by focusing on the stresses at the edge calculated by finite element method(FEM). FEM can be used for many engineering applications conveniently [17-19].They found that the ISSF at the interface corner of two-dimensional butt joint decreases with decreasing the adhesive thickness. Also, Noda *et al* [20] obtained the critical ISSF for Suzuki's experimental specimen by using two-dimensional butt joint models, and found that the adhesive strength σ_c can be evaluated as a constant critical ISSF ($K_{\sigma c} = const$) for carbon steel/epoxy resin. In this paper, by considering real specimen 3D geometry, the ISSFs on the interface outer edges of 3D butt joints will be analysed by varying the adhesive thicknesses to confirm the validity of previous 2D modelling. The reference solution in figure 1(b) will be studied under arbitrary material combinations.

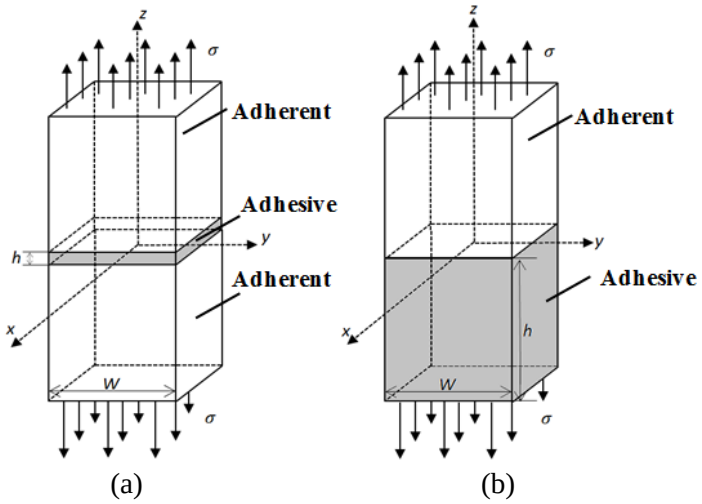

Figure 1. Three-dimensional butt joint when $h/W = 0.01\,(a)$ and $h/W = 1.0\,(b)$.

2. Three-dimensional mesh-independent technique to obtain ISSF

The most popular ISSF is known as the stress intensity factor for cracks. To obtain more general ISSF for evaluating interface strength, several analytical techniques were applied [21-28]. One of the most used numerical modelling techniques is the finite element method, which can be used for many engineering applications conveniently [29-35]. In order to obtain the ISSF, a mesh-independent technique was proposed for two-dimensional butt joints. The details are indicated in [15,16,20].

By considering the real specimen geometry, in this study, 3D butt joint as shown in figure 1(a) will be analysed. In order to apply the mesh-independent technique to 3D problem, a reference 3D solution is necessary. Therefore, 3D butt join for $h/W = 1.0$ as shown in figure 1(b) is analysed under arbitrary material combinations. Then, the adhesively bonded specimen used by Suzuki [13] is considered as comparison.

At this stage, the elastic properties for the materials are assumed as Young's modulus E=210 GPa and Poisson's ratio v=0.3 for S35C, and E=3.14 GPa and v=0.37 for epoxy resin [13]. Figure 2 shows that in the interior interface area $0 \le x, y < 0.45$ the accurate FEM stress is obtained as $|\sigma_z - 1| < 0.002$ independent of the mesh size. However, the FEM stress values near the outer of interface sides are inaccurate since they are different depending on the mesh size due to the existence of the singular stress field along the outer interface side. Focusing on the outer interface side from *y=0* to *y=W/2* (see table 1), the constant FEM stress decreases first as shown in figure 2 and then increases rapidly when *y* is close to the outer interface corner. This is because another stronger singular stress field exists around the outer interface corner. In this paper, the ISSF distribution along the outer interface side in the three-dimensional joint will be focused.

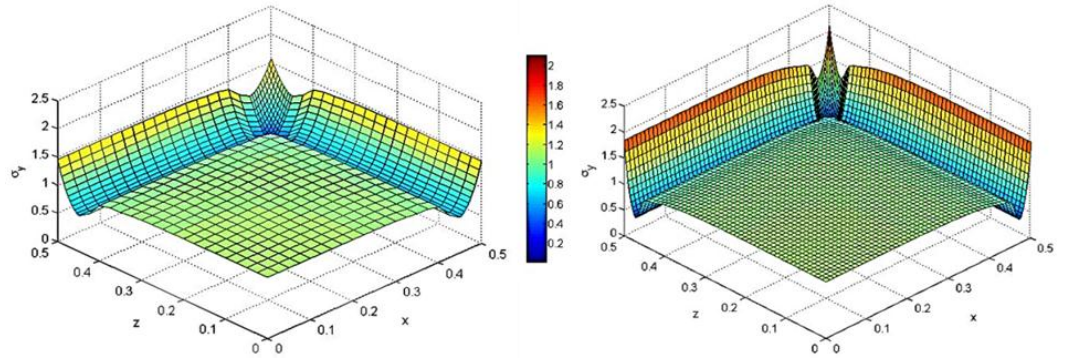

$|\sigma_z - 1| < 0.002$ on $0 \le x, y < 0.45$
(a) e_{min}=0.05

$|\sigma_z - 1| < 0.002$ on $0 \le x, y < 0.45$
(b) e_{min}=0.025

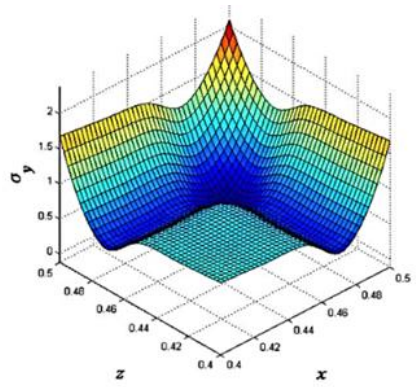

(c) Detail of x, y=0.4~0.5

Figure 2. FEM stress distribution σ_z of three-dimensional butt joint on $z = \pm h/2$ when $E_1 = 210\text{GPa}$, $\nu_1 = 0.3, E_2 = 3.14\text{GPa}$, $\nu_2 = 0.37$.

Table 1. FEM stress distributions for three-dimensional joint under tension obtained by different mesh sizes when E_1=210 GPa, ν_1=0.3, E_2=3.14 GPa and ν_2=0.37.

y	Minimum mesh size e_{min}=1/3200 around the edge			Minimum mesh size e_{min}=1/12800 around the edge		
	$\sigma^{3D}_{y,h/W=0.01}$	$\sigma^{3D}_{y,h/W\ge1}$	$\frac{\sigma^{3D,FEM}_{y,h/W=0.01}}{\sigma^{3D,\text{FEM}}_{y,h/W\ge1}}$	$\sigma^{3D}_{y,h/W=0.01}$	$\sigma^{3D}_{y,h/W\ge1}$	$\frac{\sigma^{3D}_{y,h/W=0.01}}{\sigma^{3D}_{y,h/W\ge1}}$
0.000	3.282	13.006	0.252	4.941	19.540	0.253
0.053	3.282	12.991	0.253	4.939	19.513	0.253
0.105	3.283	12.978	0.253	4.939	19.498	0.253
0.158	3.284	12.956	0.253	4.941	19.471	0.254
0.211	3.285	12.931	0.254	4.942	19.418	0.255
0.263	3.287	12.908	0.255	4.945	19.390	0.255
0.316	3.290	12.900	0.255	4.950	19.382	0.255
0.368	3.294	12.944	0.254	4.957	19.444	0.255
0.421	3.303	13.129	0.252	4.970	19.718	0.252
0.447	3.311	13.374	0.248	4.982	20.082	0.248
0.474	3.302	13.933	0.237	4.968	20.931	0.237
0.500	4.483	31.002	0.145	7.538	52.086	0.145

Table 1 shows the FEM stress distribution along the outer interface side in three-dimensional butt joint for $h/W=0.01$ and $h/W\geq 1$. It is seen that the FEM stress $\sigma_{y,h/W=0.01}^{3D}$ and $\sigma_{y,h/W\geq 1}^{3D}$ are inaccurate since they are different depending on the mesh size. However, the FEM stress ratio $\sigma_{y,h/W=0.01}^{3D}/\sigma_{y,h/W\geq 1}^{3D}$ is very accurate since they are the same independent of the mesh size. Therefore, for example, by focusing on the middle point of the side, the ISSF ratio can be expressed as the FEM stress ratio as shown in equation (1) [15,16,20].

$$\frac{K_\sigma^{3D}}{K_\sigma^{REF}}=\frac{F_\sigma^{3D}\sigma_z^\infty W^{1-\lambda}}{F_\sigma^{REF}\sigma_z^\infty W^{1-\lambda}}=\frac{\lim_{r\to 0}\left[r^{1-\lambda}\times\sigma_z^{3D,Real}(r)\right]}{\lim_{r\to 0}\left[r^{1-\lambda}\times\sigma_z^{REF,Real}(r)\right]}=\lim_{r\to 0}\left[\frac{r^{1-\lambda}\times\sigma_z^{3D,FEM}(r)}{r^{1-\lambda}\times\sigma_z^{REF,FEM}(r)}\right]=\frac{\sigma_z^{3D,FEM}(0)}{\sigma_z^{REF,FEM}(0)} \quad (1)$$

To discuss the ISSF distribution along the outer interface side, 3D butt joint in figure 1(b) is considered as the new reference solution in the next section under arbitrary material combination. The singularity index along the outer interface side can be obtained from equation (2).

$$\left[\sin^2\left(\frac{\pi}{2}\lambda\right)-\lambda^2\right]^2\beta^2+2\lambda^2\left[\sin^2\left(\frac{\pi}{2}\lambda\right)-\lambda^2\right]\alpha\beta+\lambda^2\left[\lambda^2-1\right]\alpha^2+\frac{\sin^2(\lambda\pi)}{4}=0 \quad (2)$$

Here, α and β are the Dundurs' composite parameters defined by the shearing modulus and Poisson's ratio as

$$\alpha=\frac{G_1(\kappa_2+1)-G_2(\kappa_1+1)}{G_1(\kappa_2+1)+G_2(\kappa_1+1)},\qquad \beta=\frac{G_1(\kappa_2-1)-G_2(\kappa_1-1)}{G_1(\kappa_2+1)+G_2(\kappa_1+1)} \quad (3)$$

where

$$\kappa_j=\begin{cases}\dfrac{3-\nu_j}{1+\nu_j}\ (plane\ stress)\\ 3-4\nu_j\ (plane\ strain)\end{cases}\ (j=1,2). \quad (4)$$

3. The ISSF of 3D reference solution under arbitrary material combinations

By using the similar mesh-independent technique described in section 2, the reference solution in figure 1(a) can be obtained. Figure 3 shows the ISSF ratio of the reference solution obtained from figures 1(b) and 1(b) with fixed displacement in the y-direction (plane strain 2D bonded plate). Here, 2D ISSF K_σ^{2D} was accurately obtained and indicated in [15,16,20]. In figure 3, the maximum ISSF ratio $K_\sigma^{3D}(W/2)/K_\sigma^{2D}(W/2)$ is shown under fixed (α,β) because (α,β) cannot totally control 3D ISSF [19]. For $-0.45\leq\beta\leq 0.45$, the ISSF ratio is in the range $0.537\leq K_\sigma^{3D}(W/2)/K_\sigma^{2D}(W/2)\leq 1.90$.

4. The critical ISSF distribution and critical ISSF of three-dimensional butt joint

The critical ISSF distributions are obtained when the debonding occurs for Suzuki's specimen [13] where the adherents S35C are bonded by adhesive epoxy as shown in figure 1(a). Figure 4 shows the normalized critical ISSF distributions for various h. The critical ISSF distributions are nearly the same for different adhesive thickness h. Figure 5 shows the critical ISSF $K_{\sigma c}^{3D}$ focusing on the middle point y=0 of the outer interface side. The experimental observation shows the debonding starts from the outer interface corner, but the debonding strength can be expressed as a constant critical ISSF $K_{\sigma c}^{3D}(0)$. Figure 5 coincides with the results obtained by using 2D model [20].

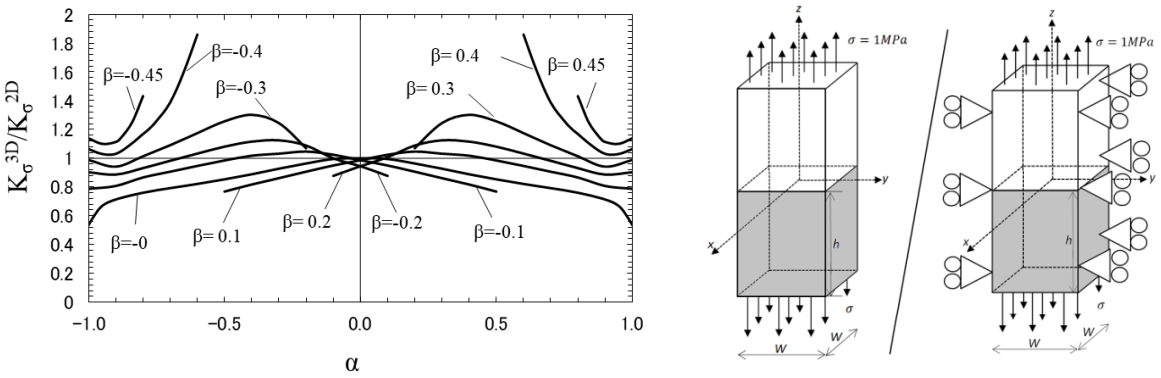

Figure 3. The maximum values of $K_\sigma^{3D}(W/2)/K_\sigma^{2D}(W/2)$ for various (α,β).

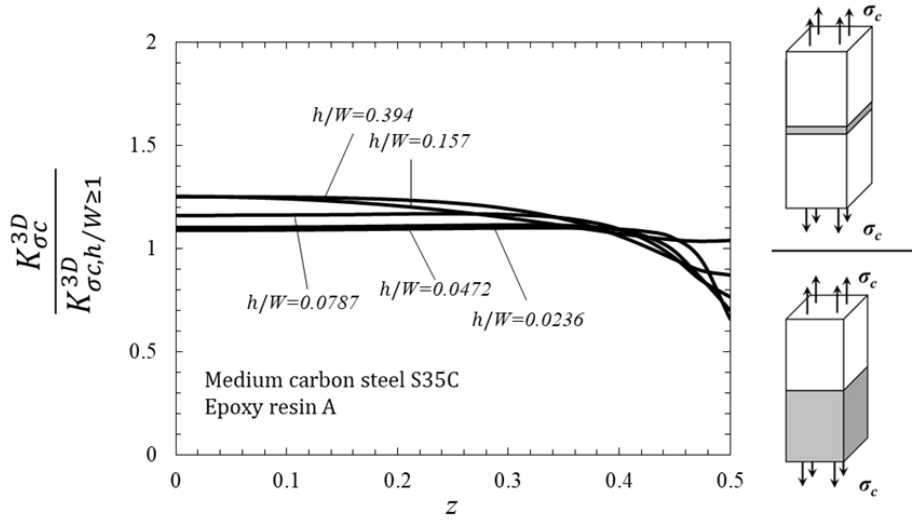

Figure 4. Critical ISSF distribution on the outer edge of the three-dimensional butt joint.

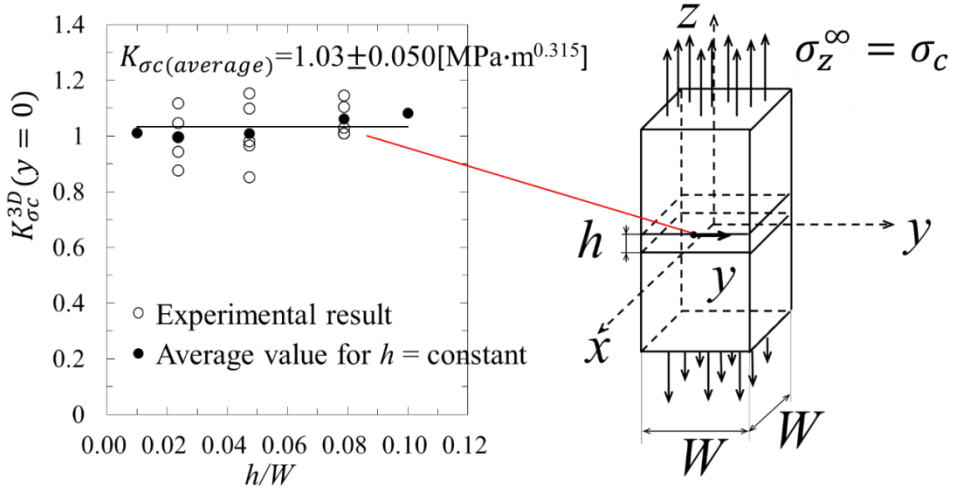

Figure 5. Constant critical ISSF focusing on (y=0).

5. Conclusion

In this study, the three-dimensional butt joint has been analyzed in terms of the intensity of singular stress field. Without considering any defects and residual strain, the elastic and homogenous adhesive is assumed to evaluate the debonding strength. The FEM stress distributions of three-dimensional butt joint are obtained by using different mesh sizes. The results show that FEM stress ratio remains constant near the middle of the outer interface side which is independent of element size. Also, the critical constant ISSF $K_{\sigma c}^{3D} = const$ can be used to express the adhesive strength by focusing on the middle point on the outer interface side. The validity of 2D modelling is confirmed since 3D results coincide with the results obtained by using 2D butt joint model [20].

References

[1] Di Pisa C and Aliabadi M H 2013 An efficient BEM formulation for analysis of bond-line cracks in thin walled aircraft structures *Int. J. Fract.* **179** 129–45
[2] Hasebe N and Kato S 2014 Solution of problem of two dissimilar materials bonded at one interface subjected to temperature *Arch. Appl. Mech.* **84** 913–31
[3] Krishnan A and Xu L R 2013 An experimental study on the crack initiation from notches connected to interfaces of bonded bi-materials Eng *Fract. Mech*. **111** 65–76
[4] Naito K, Onta M and Kogo Y 2012 The effect of adhesive thickness on tensile and shear strength of polyimide adhesive *Int. J. Adhes. Adhes*. **36** 77–85
[5] Hibino Y 1990 Influence of types and surface treatment of dental alloy and film thickness of cements on bond strength of dental luting cement *J. Japanese Soc. Dent. Mater. Dev*. **9** 786–805 (in Japanese)
[6] Asada B, Shinya A and Yokozuka S 1990 Effect of dental adhesive film thickness on bond strength *Adhes. Dent*. **8** 201–26 (in Japanese)
[7] Kagawa F, Yamada J, Suzuki T, Hisamitsu H and Wakumoto S 1991 The relationship between film thickness of resin luting cements and bond strength with the influence of thermal stress *Japan J. Conserv. Dent.* **34** 392–8 (in Japanese)
[8] Ikegami K, Kajiyama M, Kamiko S and Shiratori E 1979 Experimental studies of the strength of an adhesive joint in a state of combined stress *J. Adhes.* **10** 25–38
[9] Yamato T, Shirahama M and Hara S 1957 Effect of adhesive thickness on the strength of chlorinated rubber adhesive *J. Soc. Rubber Sci. Technol*. **30** 842–7 (in Japanese)
[10] Yokoyama T, Nakai K and Ikeda T 2006 Effect of specimen geometry on tensile properties of structural adhesive butt joints In: JSME Annual Meeting pp 861–2 (in Japanese)
[11] Akinmade A O and Nicholson J W 1995 Effect of adhesive layer thickness on the bond strength of a zinc polycarboxylate dental cement *Biomaterials* **16** 149–54
[12] Vallée T, Correia J R and Keller T 2010 Optimum thickness of joints made of GFPR pultruded adherends and polyurethane adhesive *Compos. Struct.* **92** 2102–8
[13] Suzuki Y 1987 Adhesive tensile strengths of scarf and butt joints of steel plates (relation between adhesive layer thicknesses and adhesive strengths of joints) *JSME Int. J.* **30** 1042–51
[14] Akisanya A R and Meng C S 2003 Initiation of fracture at the interface corner of bi-material joints *J. Mech. Phys. Solids.* **51** 27–46
[15] Zhang Y, Noda N A, Takaishi K and Lan X 2010 Effect of adhesive thickness on the intensity of singular stress at the adhesive dissimilar joint *J. Solid Mech. Mater. Eng*. **10** 1467–79
[16] Zhang Y, Noda N A, Wu P Z and Duan M L 2015 A mesh-independent technique to evaluate stress singularities in adhesive joints *Int. J. Adhes. Adhes.* **57** 105–17 (the corrigendum of authorship is published in *Int. J. Adhes. Adhes.* **60**(2015))
[17] Noda N A, Chen X, Sano Y, Wahab M A, Maruyama H and Fujisawa R 2016 Effect of pitch difference between the bolt–nut connections upon the anti-loosening performance and fatigue life *Mater. Des*. **96** 476-89.
[18] Miyazaki T, Noda N A, Ren F, Wang Z, Sano Y and Iida K 2017 Analysis of intensity of

singular stress field for bonded cylinder and bonded pipe in comparison with bonded plate *Int. J. Adhes. Adhes*. **77** 118-37

[19] Noda N A, Suryadi D, Kumasaki S, Sano Y and Takase Y 2015 Failure analysis for coming out of shaft from shrink-fitted ceramic sleeve *Eng. Fail. Anal.* **57** 219-35

[20] Noda N A, Miyazaki T, Li R, Uchikoba T, Sano Y and Takase Y 2015 Debonding strength evaluation in terms of the intensity of singular stress at the interface corner with and without fictitious crack *Int. J. Adhes. Adhes.* **61** 46–64

[21] Shibutani T 2004 Evaluation of crack initiation at interfacial edge on the basis of fracture mechanics concept and application to electronics devices *J. Jpn Inst. Electronics Packag.* **7** 639-44 (in Japanese)

[22] Hattori T, Sakata S, Hatsuda T and Murakami G 1988 A stress singularity parameter approach for evaluating adhesive strength *JSME Int. J. Ser. 1 Solid Mech. Strength Mater.* **31** 718–23

[23] Shiratori M 1994 Problems of joints in packaging of electronic devices *Trans. Japan Soc. Mech. Eng. A.* **60** 1905-12 (in Japanese)

[24] Kitamura T, Shibutan T and Ueno T 2002 Crack initiation at free edge of interface between thin films in advanced LSI *Eng. Frac. Mech.* **69** 1289-99

[25] Shibutani T, Tsuruga T, Yu Q and Shiratori M 2003 Criteria of crack initiation at edge of interface between thin films in opening an sliding modes for an advanced LSI *Trans. Japan Soc. Mech. Eng. A.* **69** 1368-73 (in Japanese)

[26] Takahashi Y, Aihara K, Ashida I, Niguchi K, Yamamoto Y, Arai S, Muto S and Tanaka N 2016 Evaluation of interfacial fracture strength in micro-components with different free-edge shape *Mech. Eng. J.* doi: 10.1299/mej.16-00108

[27] Hirakata H, Takahashi Y, Matsumoto S and Kitamura T 2006 Dominant stress region for crack initiation at interface edge of microdot on a substrate *Eng. Frac. Mech.* **73** 2698-709

[28] Noda N A and Takase Y 2003 Generalized stress intensity factors of V-shaped notch in a round bar under torsion, tension, and bending *Eng. Fract. Mech.* **70** 1447-66

[29] Noda N A, Suryadi D, Kumasaki S, Sano Y and Takase Y 2015 Failure analysis for coming out of shaft from shrink-fitted ceramic sleeve *Eng. Fail. Anal.* **57** 219-35

[30] Noda N A, Uchikoba T, Ueno M, Sano Y, Iida K, Wang Z and Wang G 2015 Convenient debonding strength evaluation for spray coating based on intensity of singular stress *ISIJ International* **55** 2624-30.

[31] Noda N A, Chen X, Sano Y, Wahab M A, Maruyama H and Fujisawa R 2016 Effect of pitch difference between the bolt–nut connections upon the anti-loosening performance and fatigue life *Mater. Des.* **96** 476-89

[32] Noda N A, Shen Y, Takaki R, Akagi D, Ikeda T, Sano Y and Takase Y 2017 Relationship between strain rate concentration factor and stress concentration factor *Theor. Appl. Fract. Mec.* **90** 218–27

[33] Wang Z, Noda N A, Ueno M and Sano Y 2016 Optimum design of ceramic spray coating evaluated in terms of intensity of singular stress field *Steel Research International* **88** doi: 10.1002/srin.201600353.

[34] Miyazaki T, Noda N A, Ren F, Wang Z, Sano Y and Iida K 2017 Analysis of intensity of singular stress field for bonded cylinder and bonded pipe in comparison with bonded plate *Int. J. Adhes. Adhes.* **77** 118-37

[35] Noda N A, Miyazaki T, Li R, Uchikoba T and Sano Y 2015 Dedbonding strength evaluation in terms of the intensity of singular stress at the interface corner with and without fictitious crack *Int. J. Adhes. Adhes.* **61** 46-64